Compact Dual-Band, Wide-Angle, Polarization-Angle-Independent Rectifying Metasurface for Ambient Energy Harvesting and Wireless Power Transfer

Long Li, *Senior Member, IEEE,* Xuanming Zhang, Chaoyun Song, *Member, IEEE,* Wenzhang Zhang, Tianyuan Jia, and Yi Huang, *Senior Member, IEEE*

***Abstract*— A dual-band and polarization-angle-independent rectifying metasurface (MS) with a miniaturized dimension and a wide incident angle range are presented in this article. The proposed structure consists of a single layer of periodic cell arrays with integrated diodes, a *dc* feed, and a load. A novel method of incorporating surface-mount components (e.g., diodes) into the texture is developed to simplify the structure. The matching network between MS and the nonlinear rectifier can be eliminated directly due to the multimode resonance and adjustable high-impedance characteristics of the MS. Moreover, the proposed MS can maintain high conversion efficiency by using different diodes without changing the overall topology. In addition, the proposed design can effectively capture incoming waves with arbitrary polarizations and a wide incident angle range of 60°. The 4 × 4 MS array is fabricated and measured. Experimental results show that the proposed structure can achieve maximum efficiency of 58% at 2.4 GHz and 50% at 5.8 GHz with an input power of 0 dBm under different polarizations and incident angles. Importantly, it is also shown that the rectifying MS can maintain high efficiency over a wide power range from −3 to 10 dBm. The proposed design concept is very suitable for the adaptive wireless power supply of portable devices.**

***Index Terms*— Ambient energy harvesting, integration, polarization-angle-independent, rectifying metasurface (MS), wide incident angle, wireless power transfer (WPT).**

I. Introduction

WIRELESS power transfer (WPT) technology realizes over-the-air transmission of energy and has received extensive attention in the industrial and commercial fields over the past several decades [1]. The types of WPT can be mainly divided into electromagnetic induction or coupled resonance in the near-field region and radiation or beam in the far-field region. As a new technical method of energy replenishment, WPT is theoretically more flexible and convenient than traditional physical wiring and manual replacement of power sources. With the continuous development of WPT in theory and products, energy harvesting technology has been widely studied in low-power applications in recent years [2]. So far, the energy sources that can be collected are mainly classified into solar energy, piezoelectric energy, mechanical energy, wind energy, electromagnetic energy, and so on. For WPT and wireless energy harvesting, the most popular industrial and commercial applications are: 1) wireless charging of mobile phones and electric vehicles (EVs); 2) RFID; 3) power supply of Internet of Things (IoT); 4) implantable/wearable devices; and 5) smart home. With the commercialization of 5G technologies in more countries, a surging number of terminal devices or IoT sensor nodes are developing toward large-scale, intelligent, and miniaturized, which means that the Internet of Everything will become possible.

On the other hand, an upsurge of research activities has been focused on metamaterials both theoretically and experimentally from the beginning of this century, and many new ideas and potential applications have been generated. The electromagnetic metasurface (MS) is generally a 2-D or quasi-2-D metamaterial structure, which is composed of subwavelength elements arranged periodically in a specific plane or curved surface, and its thickness is less than the operating wavelength [3]. The MS has a wide variety of applications due to its excellent characteristics of managing electromagnetic waves, such as antenna design [4], reflectarray [5], electromagnetic bandgap (EBG) structure [6], frequency-selective surface (FSS) [7], absorber [8], WPT, and energy harvesting [5], [7], [9]–[21].

The rectifying antenna (rectenna) is very important for WPT and wireless energy harvesting applications. In a common rectenna system, it typically consists of an antenna, a matching network, a rectifying main circuit with semiconductor tubes (e.g., diodes and transistors), a filter, and a load [22]–[26]. The overall performance of the rectenna is mainly represented by the characteristics of the antenna and the efficiency of the rectifying circuit. Recent reports showed that rectennas have evolved toward high-efficiency, multiband, broadband,

Manuscript received May 14, 2020; revised August 2, 2020, September 11, 2020, and November 1, 2020; accepted November 5, 2020. This work was supported by the National Key Research and Development Program of China. *(Long Li and Xuanming Zhang contributed equally to this work.) (Corresponding author: Long Li.)*

Long Li and Xuanming Zhang are with the Key Laboratory of High Speed Circuit Design and EMC of Ministry of Education, Collaborative Innovation Center of Information Sensing and Understanding, School of Electronic Engineering, Xidian University, Xi'an 710071, China (e-mail: lilong@mail.xidian.edu.cn).

Chaoyun Song, Wenzhang Zhang, Tianyuan Jia, and Yi Huang are with the Department of Electrical Engineering and Electronics, University of Liverpool, Liverpool L69 3BX, U.K. (e-mail: yi.huang@liverpool.ac.uk).

Color versions of one or more figures in this article are available at https://doi.org/10.1109/TMTT.2020.3040962.

Digital Object Identifier 10.1109/TMTT.2020.3040962

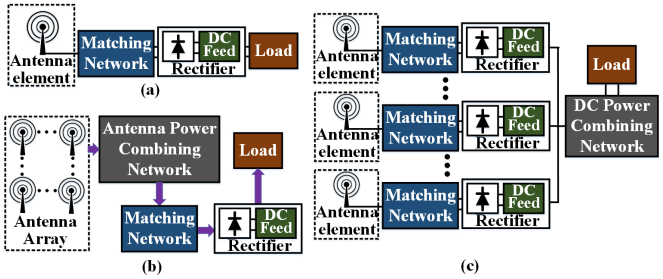

Fig. 1. Configuration of (a) general single rectenna system, (b) traditional first-combined and last-rectified rectenna array system, and (c) conventional first-rectified and last-combined rectenna array system.

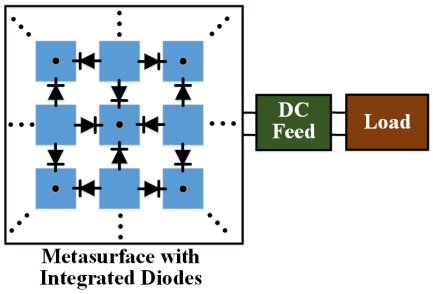

Fig. 2. Framework of the proposed rectifying MS system.

wide input-power range adaptability, and large-scale arrays [22]–[30]. To improve the performance of rectennas, MS has been reported as an energy harvester instead of the antenna in some kinds of studies [9]–[15]. The MS array for energy harvesting has gotten advantages in terms of high-efficiency, subwavelength, polarization-independent, wide angle, and conformal. However, most state-of-the-art studies on MS array with rectifying function are polarization-dependent and of a single narrowband, while the structure of RF or dc combination network is very complex, which may introduce additional loss, lower efficiency, and worse impedance matching [14], [21]. The future trend of MS structure for WPT and ambient energy harvesting is miniaturization, self-adapting, programming, and digitalization [31]. On the other hand, the rectenna arrays have also been reported to obtain preferable performance of receiving power and efficiency in the recent works of the literature [26]–[30]. At present, the performance of the rectenna arrays for directional and high input power at a single operating band is promising, but the size of the rectenna array is too large to be suitable for miniaturized applications. For the wireless power supply of miniaturized terminal devices or sensors, it is necessary for the receiver to capture energy efficiently in various environments. Therefore, an ideal receiver can harvest energy from arbitrarily polarized and randomly incident-angle electromagnetic waves and, simultaneously, has the characteristics of miniaturized, concealed, and conformal. These demands remain a challenge for the literature now reported.

The commonly adopted system configurations of a single rectenna and the rectenna arrays are shown in Fig. 1. Due to the nonlinearity of the semiconductor, the input impedance of the rectifier varies with the change of topology, load impedance, diode type, input power range, frequency, and so on, but most of the cases present high input impedance [24], [25]. Furthermore, the input impedance of the antenna introduced in most rectenna systems is 50 Ω. Whether it is a single rectenna or a rectenna array, the matching network between the antenna and the rectifier is required to conjugate match the input impedance of the nonlinear rectifying circuit with 50 Ω of the antenna impedance. Improved dynamic matching networks for different input power, load impedance, and frequency have been proposed for rectennas in previous work [23], [25], [32]–[34]. To simplify the system, some studies pay attention to high-impedance antennas and filtering-antenna designed to eliminate matching networks recently [24], [25].

In a typical array rectenna, two configurations are widely introduced, as illustrated in Fig. 1(b) and (c). The detailed configurations have been discussed in [13], [21], and [26]–[30].

1) One is first-combined and last-rectified, that is, the RF power received by rectenna arrays is combined first and then rectified into dc, as depicted in Fig. 1(b).
2) Another is first-rectified and last-combined, that is to say, a rectifying circuit is connected to antenna arrays first before dc combined, as shown in Fig. 1(c).

For the existing array rectenna designs, however, additional RF or dc power combining networks and matching networks are required for all of the abovementioned configurations. Furthermore, as the antenna array increases in scale, the design of a matching network for adapting to different impedance ranges is quite challenging, and the power combining network is large and complicated, which may lead to greater loss, higher cost, and mismatch problems.

In this article, we propose a novel compact wide-angle and polarization-angle-independent rectifying MS (RMS) array design in dual bands. The framework of the RMS system is illustrated in Fig. 2. Our configuration is made up of just three parts, namely, an MS periodic array with integrated diodes, wherein the diodes are used to rectify RF into dc and connect each cell integrally, a dc filter for smoothing waveform and eliminating the ac component, and a load. Since the MS has a strong resonance and various operating modes at the working bands, it is easier to obtain adjustable high-impedance property than the antenna. Therefore, the matching network between the proposed MS and the input impedance of the nonlinear rectifying diode can be directly eliminated. Meanwhile, through a proper combination of the MS unit cells and diodes, the MS array can be integrated completely without the need for RF or dc power combining network and, thereby, enables the simple and compact design of the RMS. Also, the design of the proposed MS energy harvester could achieve a wide range of incident angles and insensitive polarization while maintaining high harvesting efficiency. Compared with conventional rectennas, the proposed RMS has outstanding performance in terms of its compact and simple structure and low cost for manufacture. It can also adapt to a various range of input power and even different diodes, making it very suitable for self-adaptive power supply requirements of miniaturized IoT sensors.

Above all, the detailed design stages and analysis of the proposed RMS are presented in Section II. Next, the measurement and validation of the fabricated model are demonstrated

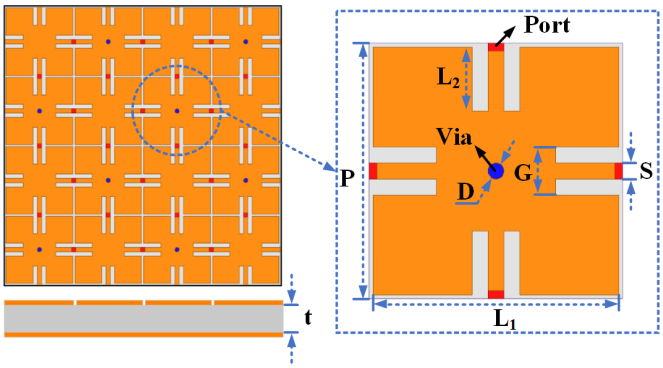

Fig. 3. Geometry of the proposed rectifying MS.

in Section III. In the end, Section IV is the performance comparison, and conclusions are given in Section V.

II. Metasurface Analysis and Design

A. Metasurface Cell Design

There are many types of MSs proposed for energy harvesting, such as the split-ring resonator (SRR), the electric-inductive-capacitive (ELC) resonator, and the butterfly-shaped closed-ring (BCR), which maintains high energy capture efficiency at their operating frequency, but most of them do not have the rectification [9]–[12], [15]. To the best of our knowledge, there are very few works in the literature regarding the MS with rectified function and good performance [21], [35]. Also, the rectified MS array in previous work certainly needs to be equipped with a large complex power combining networks (e.g., >64 units) for channeling power completely and reducing impedance mismatch [13], [36]. As a result, such designs would increase losses, costs, manufacturing errors, and nonlinear effects to decrease overall efficiency.

Moreover, due to the input impedance of nonlinearly rectifying circuit is mostly complex high impedance according to the literature, it's real part is >200 and – 500 Ω and the imaginary part is <500 Ω, which is very sensitive to the variety of input power range, frequency band, load, and diode type [22]–[25]. The MS is easier to obtain high-impedance characteristics than the antenna, which can be more suitable for the conjugate-matched rectifying circuit to eliminate matching network at the interested band and wide power range [6], [9], [11], [37].

To integrate the design of the MS and rectifying circuit completely, we introduce an MS structure, as shown in Fig. 3. The idea of the proposed geometric shape originates from the uniplanar compact photonic bandgap (UC-PBG) [6]. The UC-PBG unit cell is composed of a square metal patch and four metal wires connecting each edge center of the patch. Thus, as an equipotential surface, each unit cell in the UC-PBG array structure is directly connected. The UC-PBG structure has a broad stopband, which can be widely utilized over the microwave to the optical band. However, the goal of the proposed MS is energy harvesting. Inspired by the UC-PBG, the proposed structure is a 2-D square plane periodic array with each element similarly composed of the square metal pad with a length of L_1 and two pairs of connecting branches with a width of S in a single-layer grounded dielectric substrate.

TABLE I
Summary of MS Geometry

Parameter	Description	Value (mm)
D	The diameter of metal via at the center of MS cell	1
G	Width of the gap between the square metal pad and four connecting branches	3
L_1	Length of the square metal pad	15.5
L_2	Length of the gap between the square metal pad and four connecting branches	4
P	Period of MS unit cell	16
S	Width of four connecting branches	1
t	Thickness of substrate	1.27

The proposed MS with UC-PBG structure has the impedance ports that are connected in series through the metal branches in the middle of each adjacent element instead of being directly connected in the conventional UC-PBG. These impedance ports could conjugate match with the input impedance of the rectifying diode for the integrated coplanar design of diode and the MS unit cells. It should be emphasized that the load ports are located between each cell rather than within each cell in the reported literature [27]–[29]. There is an essential difference to the equivalent circuit of the two positions of the port. The load ports are coplanar with the MS pattern to integrate the rectifier diodes and create a dc path in the overall MS, rather than channeling energy into the other layers through the shorting via of each cell in the latest reports [10]–[13]. There is a certain gap with a width of G between the square metal pad and four connecting branches at the center of each side of the metal pad in the unit cell. The gap increases the capacitance effect, and the connecting branches bring an additional inductance effect. The Rogers 3210 material is used as the substrate with a metallic ground, a relative permittivity of 10.2, and a loss tangent of 0.0027. The pattern etched on the front of the substrate is copper with a thickness of 35 μm. The period of the cell is P, and the diameter of the metal via at the center of the cell is D. All the geometric parameters marked in Fig. 3 are summarized in Table I as a design example.

The commercial software HFSS is used to simulate the behavior of the MS, and the Floquet port with periodic boundary conditions can calculate the reflection and transmission characteristics between all ports. The lumped impedance ports are adopted to connect adjacent MS unit cells. The role of these load ports is to analyze the characteristics of the energy harvesting for the proposed structure, such as harvesting efficiency and impedance matching.

The real and imaginary parts of the input impedance for the load port are depicted in Fig. 4. It can be obtained that the resonant frequencies of the MS are around 2.4 and 5.8 GHz over the range of the interested band. The real part of the input impedance at 2.4 and 5.8 GHz reaches a high-impedance state of 400 and 200 Ω, while the imaginary part is 0 Ω. In the two resonant frequencies of the MS, the real part of the input impedance varies from 0 to 400 Ω, while the imaginary part varies between −180 and 250 Ω.

The surface current distribution of the MS cell at the resonant frequencies is analyzed, as illustrated in Fig. 5.

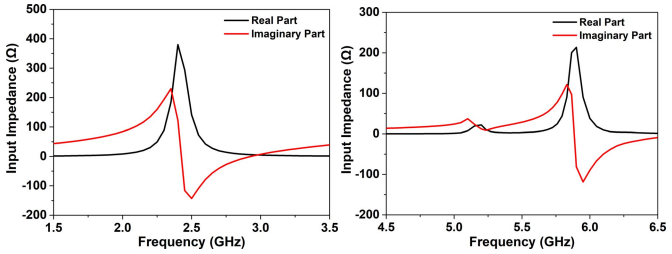

Fig. 4. Calculated the real and imaginary parts of the input impedance for the load port in two operational frequency bands.

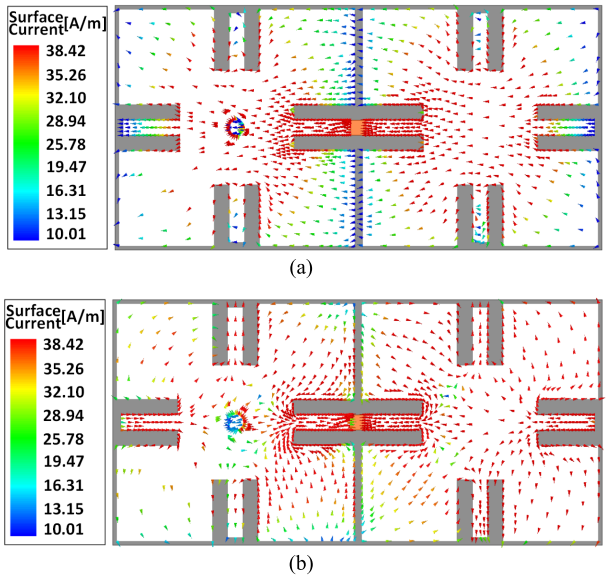

Fig. 5. Simulated surface current distributions on the MS at (a) 2.4 and (b) 5.8 GHz.

At 2.4 GHz, the surface current on each unit cell is in the same direction, which flows along the maximum path of the MS cell to generate this low-frequency resonant mode. At this point, the MS unit cell is electrically small with the period of $\lambda_1/8$ (λ_1 is the wavelength at the low resonant frequency of 2.4 GHz). Meanwhile, the surface current of adjacent elements is opposite at 5.8 GHz, and the period of the MS unit is $\lambda_2/3$ (λ_2 is the wavelength at the high resonant frequency of 5.8 GHz). Here, the size of the MS unit is no longer electrically small. In this case, the array of the MS operates in a differential mode [30]. Due to the opposite current direction of adjacent cells in the differential mode, the voltage difference on the ports between neighboring units is twice as large. For rectifying diodes integrated on the ports, it is easier to reach the turn-on voltage of the diodes at this operating frequency to improve the rectifying efficiency. As a result, the MS has two resonant frequencies with high impedance, which works in the different resonant modes.

The total energy harvesting efficiency of the MS harvester is given by [10]–[13]

$$\eta_{\text{Total}} = \eta_{\text{MS}}\eta_{\text{RF-DC}} \tag{1}$$

$$\eta_{\text{MS}} = \frac{p_{\text{MS-load}}}{p_{\text{received}}} \times 100\% \tag{2}$$

$$\eta_{\text{RF-DC}} = \frac{p_{\text{DC-Load}}}{p_{\text{MS-load}}} \times 100\% \tag{3}$$

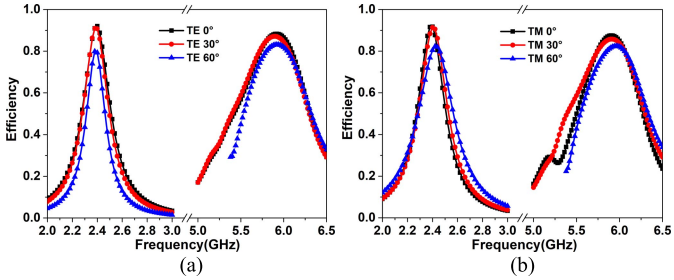

Fig. 6. Calculated harvesting efficiency of the MS at different incident angles with (a) TE polarization and (b) TM polarization.

where η_{MS} is the energy absorption efficiency of the MS harvester without rectification. $P_{\text{MS-load}}$ is the power captured by the RMS load ports, and P_{received} is the received total power incident on the overall MS, which can be calculated using the surface integral of a Poynting vector on the MS aperture area. Then, $\eta_{\text{RF-dc}}$ is the RF-dc conversion efficiency of the rectifying circuit, and $P_{\text{dc-load}}$ is the output dc power of the load.

Then, the model can be used to calculate the performance of energy harvesting efficiency by (2) under different polarization directions and incident angles. Similar to the analysis of the absorber [8], [11]–[12], the stability of the incident angle of the MS collector can be generally divided into two kinds of oblique incidence. One is transverse electric (TE) oblique incidence, and the other is the transverse magnetic (TM) oblique incidence.

Fig. 6 shows the energy collection efficiency of the MS at different incident angles with TE and TM polarizations. For the TE polarization, when the incidence angle changes from 0° to 60°, the highest collection efficiency (appearing at the resonant frequency) decreases gradually from 92% to 80% in the low-frequency resonant mode of 2.4 GHz and from 88% to 83% in the high-frequency resonant mode of 5.8 GHz, but the resonant frequency of the two bands are almost not offset. Moreover, the half-power bandwidth (HPBW) slightly reduces from 300 (in 0°) to 220 MHz (in 60°) at 2.4 GHz and from 980 (in 0°) to 880 MHz (in 60°) at 5.8 GHz. This is because the enlargement of the propagation path of the incident wave leads to the decrease in the vertical component of the wave vector with an increase in the incident angle of the TE polarization, and further effective electrical resonance is gradually reduced resulting in a slight decrease in efficiency and bandwidth. For the TM polarization, the bandwidth remains almost unchanged, but the resonance frequency shifts a little as the incident angle increases, which is due to an increase in the equivalent magnetic resonance. As a result, it still maintains a high collection efficiency (>80%) in both resonant modes despite there is a slight frequency offset or bandwidth drop under TE and TM polarizations.

Finally, we calculate the energy harvesting efficiency with and without via at the center of the unit cell of the MS shown in Fig. 7. It can be seen that there is a slight frequency offset in the case of via, and the via-free unit cell due to the introduction of via increases the equivalent inductance effect and surface current propagation path of MS structure, which results in the shift of resonant frequency, but the efficiency

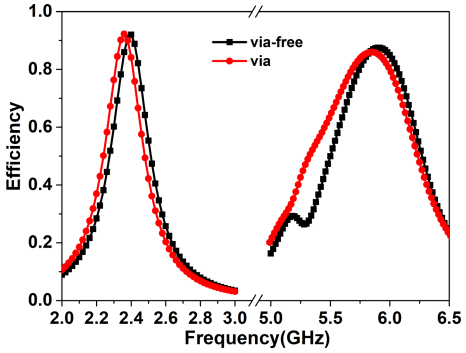

Fig. 7. Calculated harvesting efficiency with and without via at the center of the MS unit cell.

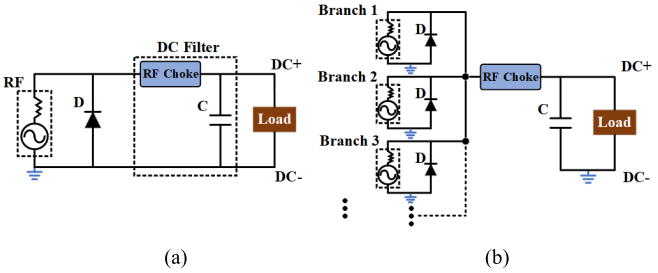

Fig. 8. Schematic of (a) single-shunt-diode rectifier circuit (class-F) and (b) single-shunt-diode rectifier circuit with multichannel parallel connection.

is still higher than 86%. This performance will be used for the MS array arrangement and circuit combinations in Sections II-B and C.

Therefore, the proposed MS element has the characteristics of high input impedance, high efficiency, a wide range of incident angles, and polarization stability in the two different operating modes designed in 2.4 and 5.8 GHz.

B. Rectifier Design

The MS structure transfers the captured space electromagnetic wave energy into the harvesting ports between the cells and generates an equivalent RF voltage source. At this time, the rectifying diodes are connected to these ports in parallel, and then, the input impedance of the proposed MS would directly match the input impedance of the rectifier circuit within the designed frequency band. Herein, a single-shunt-diode rectifier circuit (class-F) [24], [38] with a very simple schematic and high efficiency is selected and depicted in Fig. 8(a).

It can be observed that the power source is equivalent to the output port of an antenna or an energy harvester and is connected in parallel with the rectifying diode. The diodes could be normally selected according to the frequency and input power range, such as the SMS-7630 is suitable for low-power applications, the HSMS-2850 is fit for medium power applications, and the HSMS-2860 is used for high-power applications. The role of the RF choke in series is to provide a dc path while blocking the RF power, while the capacitor in parallel is to smooth waveform and store dc power. Here, the chip inductor of 47 nH and the chip capacitor of 0.1 μF are introduced for the proposed circuit design. The series inductor and shunt capacitor are equivalent to the structure of a dc filter. The load

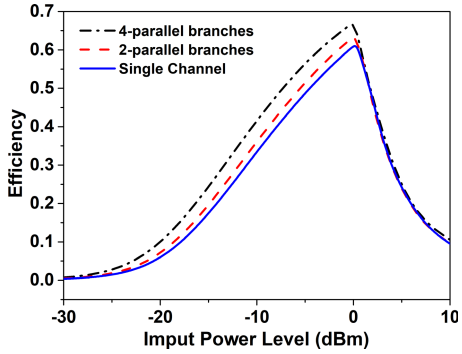

Fig. 9. Simulated efficiency of single-channel and parallel multichannel rectifier varying with the incident power at 2.4 GHz.

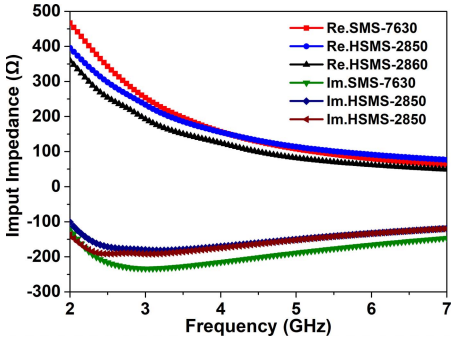

Fig. 10. Simulated input impedance of the rectifier for the different diodes. The input power levels are 0 dBm with the SMS-7630 diode, 5 dBm with the HSMS-2850 diode, and 10 dBm with the HSMS-2860 diode.

resistance of 700 Ω is used to dc power output and impedance matching adjustment.

For the rectenna array, the connection types of the rectifier circuit branches are series, parallel, and cascaded [13], [26]. To reduce ohmic losses and improve total efficiency, partial series and overall parallel connection methods are generally considered to be optimal choices in the recent reports [26]. For our proposed MS array, to integrate the design of the structure and optimize the efficiency, the rectifier circuit with the whole parallel connection is shown in Fig. 8(b).

The harmonic balance (HB) simulator of the ADS software is used for modeling the rectifier. Fig. 9 shows the simulated efficiency of single-channel and parallel multichannel rectifier versus the incident power at 2.4 GHz. Here, we choose the SMS-7630 diode as an example, and the other parameters are the same. It can be seen that the rectification efficiency increases slightly with the number of parallel channels increases, which indicates the advantage of multichannel parallel connection.

Fig. 10 shows the simulated input impedance of the rectifier as a function of frequency for the different diodes. The input impedances of the three different diodes at 2.45 and 5.8 GHz are listed in Table II. The MS port impedance could conjugate match the input impedance of the circuit using the different diodes without changing topology and dimensions.

C. Metasurface Array Design

Here, we built the RMS with a novel method of incorporating rectifying diodes into the texture, as illustrated in Fig. 11. It can be seen that the RMS array consists of via and via-free

TABLE II
INPUT IMPEDANCE OF THE RECTIFIR FOR DIFFERENT DIODES

Diode type	Input impedance		Optimal power level
	2.4 GHz	5.8 GHz	
SMS-7630	365-j*207 Ω	104-j*186 Ω	0 dBm
HSMS-2850	313-j*165 Ω	110-j*148 Ω	5 dBm
HSMS-2860	269-j*190 Ω	79-j*149 Ω	10 dBm

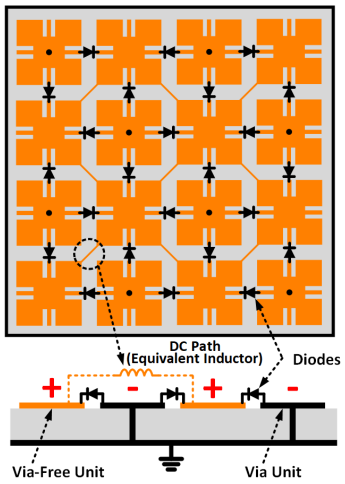

Fig. 11. Schematic of the proposed rectifying MS with a new method of incorporating rectifying diodes into the texture.

units (both the via and via-free units are half of the total number of periodic array cells) arranged alternately, and its characteristic is mentioned in Fig. 7 [37]. The four connecting branches of each via unit are connected to the positive pole of the rectifying diode, while the four connecting branches of each via-free unit are linked to the negative pole of the rectifying diode. In the periodic surface array, all via units are connected to the ground by a metal via to form an equipotential surface with the same potential as the ground, which is defined as dc−. The remaining units without via are linked by the thin metal wires that are equivalent to inductors to build dc paths while blocking the RF power; thus, another positive voltage level of dc+ is defined. More specifically, the electric potentials of each of the neighboring via and via-free units are unequal results in a potential difference across the diodes between adjacent cells. According to the topology of the parallel-type rectifier circuit mentioned in Section II-A, the positive and negative poles of the diodes are connected to the corresponding equipotential surface to develop a new arrangement mode of RMS.

Fig. 12 shows the equivalent circuit of the proposed surface arrangement by the understanding and improvement of Fig. 8(b). An equivalent RF voltage source is formed at the ports in the middle of each two adjacent cells. The impedance of the equivalent RF voltage source (equivalent to the input impedance of the port between the MS cells analyzed in Section II-B) is matched with the rectifier circuit. The main circuit of the rectifier circuit in parallel form is composed of an equivalent RF voltage source for each port in the array and a rectifying diode connected in parallel at the ends of the port. Then, the negative poles of all equivalent rectification branches

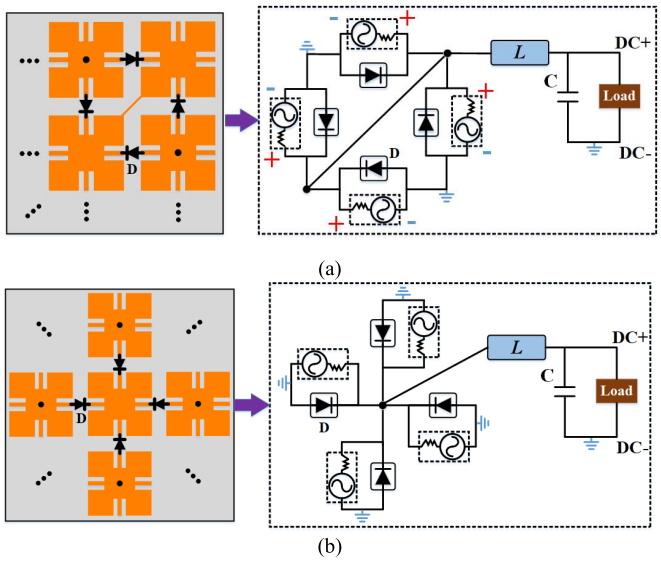

Fig. 12. (a) Part of the equivalent circuit of the proposed RMS. (b) Another part of the equivalent circuit of the proposed RMS.

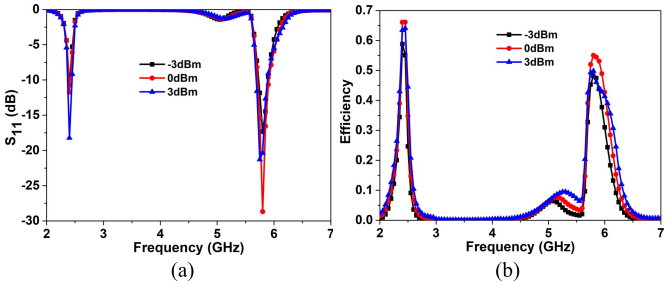

Fig. 13. (a) Simulated reflection coefficient and (b) RF-dc efficiency of the proposed RMS at different input power levels. The diode type is SMS-7630.

through the equipotential surface dc− are linked together, and the positive poles of all equivalent rectification branches are also connected in the union by the equipotential surface dc+. As a result, all the equivalent rectification branches are connected in parallel through the equipotential surface dc+ and then channeled into the class-F dc-filter uniformly to ensure the smooth output of the dc waveform and isolate the RF power from the load. Note that an increase in the number of the branch results in a decrease in the load resistance to achieve high efficiency. In this case, the total output power will become larger.

The HFSS and the ADS are used for cosimulation to understand the common effects of the field and the circuit. First, the frequency-domain power source port is adopted in the ADS as the equivalent RF voltage source on the power harvesting port between the MS unit cells. Then, the impedance of the power source port in the ADS is imported by the touchstone S1P file, which calculates in the HFSS that the input impedance of the MS varies with the frequency.

The reflection coefficient and corresponding efficiency of the proposed RMS calculated by cosimulation at the different input power levels are shown in Fig. 13(a) and (b). Note that this efficiency is the overall RF-dc conversion efficiency of η_{Total} calculated by (1) compared with the result η_{MS} calculated

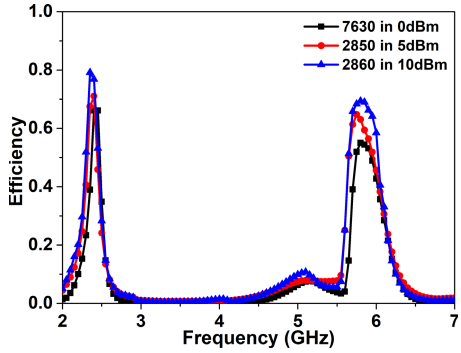

Fig. 14. Calculated RF-dc efficiency of the MS integrated with different diodes at the corresponding optimal power level.

by (2) in Fig. 6, which shows the efficiency of the MS without rectification. Since the SMS-7630 integrated into the RMS is suitable for low-power applications, the optimum input power is approximately 0 dBm due to the diode reaching its saturation voltage at this power level. It can be seen that the two resonant modes result in the total RF-dc efficiency of 66% at 2.4 GHz and 55% at 5.8 GHz with a power level of 0 dBm. Also, the result at the high-power input of 3 dBm and the low-power input of −3 dBm is added as an extension and comparison of the performance. It can be observed that the two resonant modes of the RMS keep high rectifying efficiency (>50%) in the case the input power level is doubled or halved.

Fig. 14 shows the conversion efficiency of the MS integrated with different diodes, where the diode operates at the corresponding optimal power level, and the other parameters have the same value. The input impedance of the different diodes corresponds to Fig. 10 and Table II. With an increase in the input power, the conversion efficiency of two resonant bands enlarges, and the load can be optimized to achieve the optimum conversion efficiency at the corresponding power level since the diodes for large power levels have higher reverse breakdown voltage to adapt to the rectification with high input power. Thus, the proposed RMS is a power-adaptive structure for different RF power levels without changing the structural parameters and does not require an additional matching network, which is rarely used in the latest report of the rectenna arrays. This increases the power scaling of the proposed RMS for more potential applications.

III. Measurements and Validations

A 4 × 4 array with an overall dimension of 67 mm × 64 mm × 1.27 mm was fabricated using the parameters given in Table I. The layout design and physical model of RMS are depicted in Fig. 15. It can be observed that one side of the substrate is extended by 3 mm to place the dc feed circuit (including the chip capacitor and chip inductor using the same parameters) and connected to the element located at the edge of the array where the potential of the element is dc+ in terms of the equivalent circuit, as shown in Fig. 12. This configuration formed the final RMS physical model.

Next, the measurement setup is demonstrated in Fig. 16. The whole experiment was carried out in a microwave anechoic chamber. First, the signal generator excites the RF power and then transmits it through the standard horn antenna,

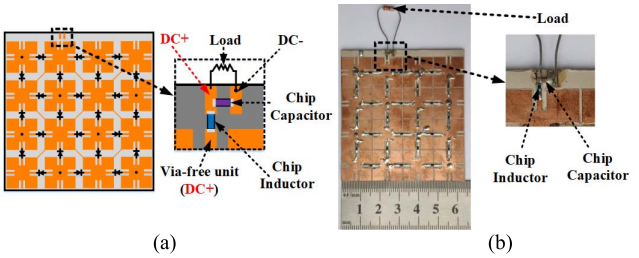

Fig. 15. Layout design and fabricated model of proposed RMS. (a) Layout design. (b) Fabricated model.

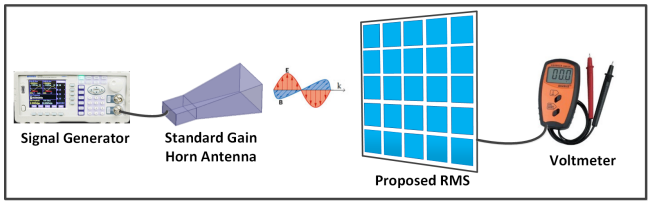

Fig. 16. Experimental setup for measuring harvesting efficiency.

which is selected to cover the tested frequency band. Then, the proposed RMS is placed in the far-field of the transmitting horn to ensure the plane wave excitation and convert the received RF power into dc. Finally, a dc voltmeter is used to measure the dc output voltage across the load resistor. Here, the measurement efficiency of energy harvesting is calculated as follows [22]–[25]:

$$\eta_{\text{measurement}} = \frac{P_{\text{load}}}{P_r} \times 100\% \tag{4}$$

where P_{load} is the output dc power, which can be written as

$$P_{\text{load}} = \frac{V_{\text{out}}^2}{R_{\text{load}}} \tag{5}$$

where V_{out} is the measured dc voltage across the load and R_{load} is the value of the load resistance. P_r is the RF power received by the RMS from the transmitting horn, which is given by [9]–[13], [27]–[29]

$$P_r = \frac{G P_{\text{input}}}{4\pi R^2} \cdot A_e \tag{6}$$

where G is the gain of a standard horn antenna and P_{input} is the input power of the transmitting horn antenna provided by a signal generator. R is the distance between the transmitting horn and the receiving RMS. A_e is the effective receiving aperture of RMS. According to previous reports [13], [27]–[29], A_e can be expressed as the physical surface area of the RMS. In the measurement, the received power P_r can be scanned within a certain power range to change the input power P_{input} by using (6). It should be noted that the simulated S-parameter, as exhibited in Fig. 13(a), cannot be directly tested because the proposed MS harvester integrates the rectifying function.

Fig. 17 shows the energy harvesting efficiency of RMS at different incident powers under normal incidence. It can be seen that the maximum measurement efficiency of RMS at 0 dBm is 58% at 2.4 GHz and 51% at 5.8 GHz compared with the simulation results of 66% at 2.4 GHz and 55% at 5.8 GHz. For 3 and −3 dBm, the maximum efficiency is 53% and 48% at 2.4 GHz and 45% and 40% at 5.8 GHz. In general, the

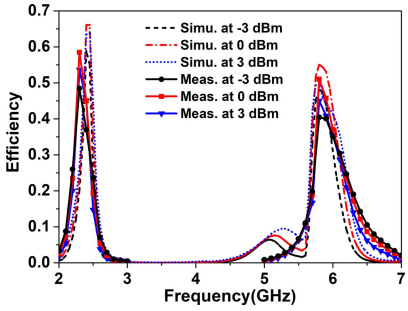

Fig. 17. Simulated and measured the energy harvesting efficiency of the fabricated RMS at different incident power levels. The diode type is SMS-7630.

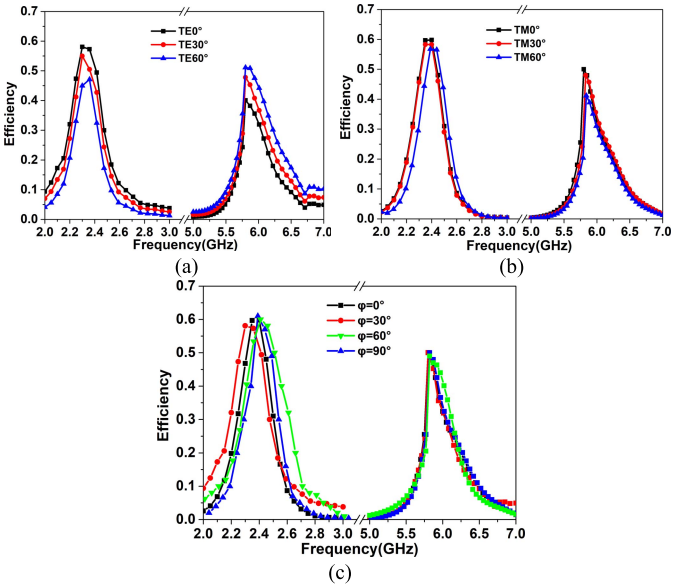

Fig. 18. Measured efficiency of the fabricated RMS for (a) TE-polarized oblique incidence, (b) TM-polarized oblique incidence, and (c) different polarization angles under normal incidence.

efficiency drop of the RMS is less than 20% in each operating band when the input power varies within a certain range.

Fig. 18(a) and (b) shows the efficiency of the RMS at different incident angles for both TE and TM polarizations. It can be obtained that the RMS has a slight frequency offset at the oblique incidence of TE and TM but has no obvious influence on the harvesting efficiency with an increase in incidence angle in the two resonant modes. Fig. 18(c) shows the conversion efficiency of the RMS at two operating frequency bands under different polarization angles. It can be obtained that the harvesting efficiency of the proposed RMS was still over 56% at 2.4 GHz and over 50% at 5.8 GHz under the different polarization angle φ. Note that this efficiency is the overall RF-dc efficiency. Compared with the simulation result in Fig. 6 that shows the efficiency of the MS without rectification, these measured results take into account the RF-dc efficiency of the whole structure. Besides, the RMS manufactured is an array of finite elements, and the simulation with an infinite period could result in slightly different results. Moreover, the nonlinearity of the diodes and the manufacturing error might also cause a small frequency offset in the experiment.

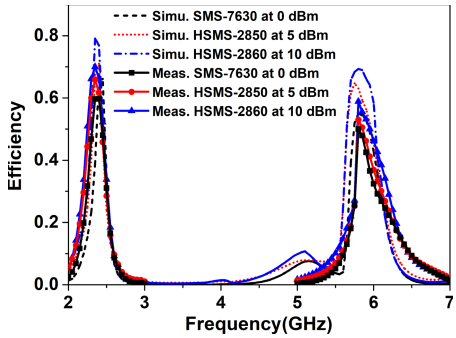

Fig. 19. Simulated and measured efficiency of the fabricated RMS using different diodes at their optimum input power.

TABLE III
RMS PERFORMANCE FOR USING DIFFERENT DIODES

Diode type	Maximum conversion efficiency				Optimal power level
	2.4 GHz Simu.	2.4 GHz Meas.	5.8 GHz Simu.	5.8 GHz Meas.	
SMS-7630	66%	58%	55%	51%	0 dBm
HSMS-2850	71%	65%	64%	53%	5 dBm
HSMS-2860	79%	70%	69%	59%	10 dBm

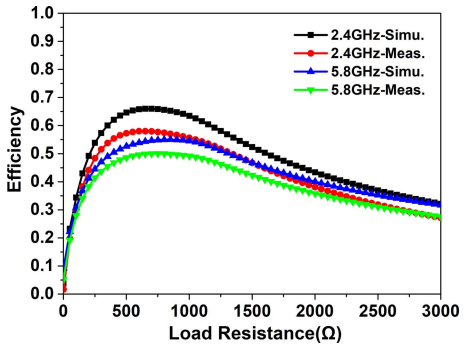

Fig. 20. Simulated and measured efficiency of the fabricated RMS versus load resistance at two operating frequencies. The input power level is 0 dBm, and the diode type is SMS-7630.

To validate the RMS in Fig. 14 for integrating different diodes, the three versions of the RMS with the same dimensions and components except for the diode are integrated with SMS-7630, HSMS-2850, and HSMS-2860, respectively. Fig. 19 shows the efficiency of the RMS using different diodes at their optimum input power. According to the results in Fig. 13(b), 14, 17, and 19, the performance of the RMS by using different diodes is shown in Table III. It can be obtained that the RMS can efficiently harvest energy in two different frequency bands at low-, medium-, and high-input powers without changing other parameters by introducing the matching diodes. Then, the conversion efficiency as the change of load resistance is simulated and measured, as shown in Fig. 20, Here, the RMS is loaded with the SMS-7630 diode, and the optimal input power is 0 dBm. It can be seen that, when the load impedance is around 700 Ω, the two working frequency bands of RMS can maintain high conversion efficiency ($>$50%) at the same time and have a certain impedance bandwidth. Simulation and experiment results verify the uniformity of the RMS.

TABLE IV
PERFORMANCE COMPARISON OF PROPOSED DESIGN AND RELATED WORKS

References (year)	Frequency (GHz)	Maximum Harvesting Efficiency		Polarization Mode	The dimension of Unit Cell (mm)	Use of Matching Network	Type of Diode & Optimal Power Level	Complexity of General Design
		Simu.	Meas.					
[14] (2017)	6.75	50% @0 dBm	Not Report	linear	30×30 (single layer)	No	Ideal (0 dBm)	Simple
[13] (2017)	3	78% @12 dBm	40% @12 dBm	linear	15×15×1.54 (dual layer)	Yes	HSMS-2860 (12 dBm)	Complex
[21] (2014)	2.18	28.81% @0 dBm	27.714% @0 dBm	linear	30×30×3.7 (dual layer)	Yes	HSMS-2828 (0 dBm)	Complex
[7] (2018)	2.45	75% @15 dBm	61% @15 dBm	linear	35×57.5×6.5 (dual layer)	Yes	HSMS-286P (15 dBm)	Complex
[28] (2018)	2.84	72% @18.75 dBm	60% @18.75 dBm	linear	50×50×3.175 (single layer)	No	HSMS-2860 (18.75 dBm)	Medium
[29] (2019)	3	94% @16 dBm	74% @16 dBm	Polarization Independent	20×20×4 (dual layer)	No	HSMS-2860 (16 dBm)	Medium
This work (2020)	Dual Band 2.4, 5.8	79%@10 dBm 2.4GHz, 69%@10 dBm 5.8GHz, 71%@5 dBm 2.4GHz, 64%@5 dBm 5.8GHz, 66%@0 dBm 2.4GHz, 55%@0 dBm 5.8 GHz	70%@10 dBm 2.4GHz, 59%@10 dBm 5.8GHz, 65%@5 dBm 2.4GHz, 53%@5 dBm 5.8GHz, 58%@0 dBm 2.4GHz, 51%@0 dBm 5.8 GHz	Polarization Angle Independent & Wide Angle	16×16×1.27 (single layer)	No	Power and diode adaptive (-3 to 10 dBm)	Simple

IV. PERFORMANCE COMPARISON

Based on the simulated and experimental results, the proposed RMS is compared with other related work, as shown in Table IV. It can be seen that the proposed RMS showed a new method of incorporating rectifying diodes into the MS texture, which can significantly reduce the complexity of the design and make the structure simpler and smaller, compared with the related work. Also, the RMS is highly efficient over a wide range of input power by using different types of diodes to make the RMS has input power tunable and adaptive without changing topologies and parameters. Due to the multimode resonance characteristics of the MS, the operating frequency of the RMS can be easily expanded to cover dual or even multiple bands. Also, RMS is wide-angle and polarization-angle-independent, making it has better self-adaptive capability in WPT and wireless energy harvesting systems.

V. CONCLUSION

A novel compact wide-angle range and polarization-angle-independent rectifying MS array with two operating frequency bands have been demonstrated in this article. Through numerous analyses, simulations, and measurements, the proposed rectifying MS has been realized by using the new concept of incorporating rectifying diodes into the texture. Moreover, it has achieved high RF-dc conversion efficiency in dual bands over a wide input power range from -3 to 10 dBm, a wide incident angle of 60°, and at different polarizations without the need of complex match networks and also without the need for tuning topologies and dimensions. The proposed MS design has achieved the advancements, such as compact size, low cost, wide-angle reception, and tunable input power range, therefore making it very suitable for the wireless power supply of miniaturized terminal devices in IoT applications.

REFERENCES

[1] N. Shinohara, "Power without wires," *IEEE Microw. Mag.*, vol. 12, no. 7, pp. S64–S73, Dec. 2011.
[2] S. Hemour and K. Wu, "Radio-frequency rectifier for electromagnetic energy harvesting: Development path and future outlook," *Proc. IEEE*, vol. 102, no. 11, pp. 1667–1691, Nov. 2014.
[3] C. L. Holloway, E. F. Kuester, J. A. Gordon, J. O'Hara, J. Booth, and D. R. Smith, "An overview of the theory and applications of metasurfaces: The two-dimensional equivalents of metamaterials," *IEEE Antennas Propag. Mag.*, vol. 54, no. 2, pp. 10–35, Apr. 2012.
[4] F. H. Lin and Z. N. Chen, "Low-profile wideband metasurface antennas using characteristic mode analysis," *IEEE Trans. Antennas Propag.*, vol. 65, no. 4, pp. 1706–1713, Apr. 2017.
[5] S. Yu, H. Liu, and L. Li, "Design of near-field focused metasurface for high-efficient wireless power transfer with multifocus characteristics," *IEEE Trans. Ind. Electron.*, vol. 66, no. 5, pp. 3993–4002, May 2019.
[6] F.-R. Yang, K.-P. Ma, Y. Qian, and T. Itoh, "A uniplanar compact photonic-bandgap (UC-PBG) structure and its applications for microwave circuit," *IEEE Trans. Microw. Theory Techn.*, vol. 47, no. 8, pp. 1509–1514, Aug. 1999.
[7] F. Erkmen, T. S. Almoneef, and O. M. Ramahi, "Scalable electromagnetic energy harvesting using frequency-selective surfaces," *IEEE Trans. Microw. Theory Techn.*, vol. 66, no. 5, pp. 2433–2441, May 2018.
[8] N. I. Landy, S. Sajuyigbe, J. J. Mock, D. R. Smith, and W. J. Padilla, "Perfect metamaterial absorber," *Phys. Rev. Lett.*, vol. 100, May 2008, Art. no. 207402.
[9] O. M. Ramahi, T. S. Almoneef, M. Alshareef, and M. S. Boybay, "Metamaterial particles for electromagnetic energy harvesting," *Appl. Phys. Lett.*, vol. 101, no. 17, Oct. 2012, Art. no. 173903.
[10] T. S. Almoneef and O. M. Ramahi, "Metamaterial electromagnetic energy harvester with near unity efficiency," *Appl. Phys. Lett.*, vol. 106, no. 15, Apr. 2015, Art. no. 153902.
[11] X. Zhang, H. Liu, and L. Li, "Tri-band miniaturized wide-angle and polarization-insensitive metasurface for ambient energy harvesting," *Appl. Phys. Lett.*, vol. 111, no. 7, Aug. 2017, Art. no. 071902.

[12] H.-T. Zhong, X.-X. Yang, C. Tan, and K. Yu, "Triple-band polarization-insensitive and wide-angle metamaterial array for electromagnetic energy harvesting," *Appl. Phys. Lett.*, vol. 109, no. 25, Dec. 2016, Art. no. 253904.

[13] M. El Badawe, T. S. Almoneef, and O. M. Ramahi, "A metasurface for conversion of electromagnetic radiation to DC," *AIP Adv.*, vol. 7, no. 3, Mar. 2017, Art. no. 035112.

[14] G. T. Oumbé Tékam, V. Ginis, J. Danckaert, and P. Tassin, "Designing an efficient rectifying cut-wire metasurface for electromagnetic energy harvesting," *Appl. Phys. Lett.*, vol. 110, no. 8, Feb. 2017, Art. no. 083901.

[15] A. Ghaneizadeh, M. Joodaki, J. Borcsok, A. Golmakani, and K. Mafinezhad, "Analysis, design, and implementation of a new extremely ultrathin 2-D-isotropic flexible energy harvester using symmetric patch FSS," *IEEE Trans. Microw. Theory Techn.*, vol. 68, no. 6, pp. 2108–2115, Jun. 2020.

[16] B. Alavikia, T. S. Almoneef, and O. M. Ramahi, "Wideband resonator arrays for electromagnetic energy harvesting and wireless power transfer," *Appl. Phys. Lett.*, vol. 107, no. 24, Dec. 2015, Art. no. 243902.

[17] H.-T. Zhong, X.-X. Yang, X.-T. Song, Z.-Y. Guo, and F. Yu, "Wideband metamaterial array with polarization-independent and wide incident angle for harvesting ambient electromagnetic energy and wireless power transfer," *Appl. Phys. Lett.*, vol. 111, no. 21, Nov. 2017, Art. no. 213902.

[18] B. Ghaderi, V. Nayyeri, M. Soleimani, and O. M. Ramahi, "Pixelated metasurface for dual-band and multi-polarization electromagnetic energy harvesting," *Sci. Rep.*, vol. 8, no. 1, p. 13227, Dec. 2018.

[19] F. Yu, X. Yang, H. Zhong, C. Chu, and S. Gao, "Polarization-insensitive wide-angle-reception metasurface with simplified structure for harvesting electromagnetic energy," *Appl. Phys. Lett.*, vol. 113, no. 12, Sep. 2018, Art. no. 123903.

[20] B. Ghaderi, V. Nayyeri, M. Soleimani, and O. M. Ramahi, "Multi-polarisation electromagnetic energy harvesting with high efficiency," *IET Microw., Antennas Propag.*, vol. 12, no. 15, pp. 2271–2275, Dec. 2018.

[21] R. Wang *et al.*, "Optimal matched rectifying surface for space solar power satellite applications," *IEEE Trans. Microw. Theory Techn.*, vol. 62, no. 4, pp. 1080–1089, Apr. 2014.

[22] C. Song, Y. Huang, J. Zhou, J. Zhang, S. Yuan, and P. Carter, "A high-efficiency broadband rectenna for ambient wireless energy harvesting," *IEEE Trans. Antennas Propag.*, vol. 63, no. 8, pp. 3486–3495, Aug. 2015.

[23] C. Song *et al.*, "A novel six-band dual CP rectenna using improved impedance matching technique for ambient RF energy harvesting," *IEEE Trans. Antennas Propag.*, vol. 64, no. 7, pp. 3160–3171, Jul. 2016.

[24] C. Song *et al.*, "Matching network elimination in broadband rectennas for high-efficiency wireless power transfer and energy harvesting," *IEEE Trans. Ind. Electron.*, vol. 64, no. 5, pp. 3950–3961, May 2017.

[25] C. Song, Y. Huang, P. Carter, J. Zhou, S. D. Joseph, and G. Li, "Novel compact and broadband frequency-selectable rectennas for a wide input-power and load impedance range," *IEEE Trans. Antennas Propag.*, vol. 66, no. 7, pp. 3306–3316, Jul. 2018.

[26] Y.-J. Ren and K. Chang, "5.8-GHz circularly polarized dual-diode rectenna and rectenna array for microwave power transmission," *IEEE Trans. Microw. Theory Techn.*, vol. 54, no. 4, pp. 1495–1502, Jun. 2006.

[27] A. Z. Ashoor, T. S. Almoneef, and O. M. Ramahi, "A planar dipole array surface for electromagnetic energy harvesting and wireless power transfer," *IEEE Trans. Microw. Theory Techn.*, vol. 66, no. 3, pp. 1553–1560, Mar. 2018.

[28] T. S. Almoneef, F. Erkmen, M. A. Alotaibi, and O. M. Ramahi, "A new approach to microwave rectennas using tightly coupled antennas," *IEEE Trans. Antennas Propag.*, vol. 66, no. 4, pp. 1714–1724, Apr. 2018.

[29] A. Z. Ashoor and O. M. Ramahi, "Polarization-independent cross-dipole energy harvesting surface," *IEEE Trans. Microw. Theory Techn.*, vol. 67, no. 3, pp. 1130–1137, Mar. 2019.

[30] T. Matsunaga, E. Nishiyama, and I. Toyoda, "5.8-GHz stacked differential rectenna suitable for large-scale rectenna arrays with DC connection," *IEEE Trans. Antennas Propag.*, vol. 63, no. 12, pp. 5944–5949, Dec. 2015.

[31] L. Li, X. Zhang, C. Song, and Y. Huang, "Progress, challenges, and perspective on metasurfaces for ambient radio frequency energy harvesting," *Appl. Phys. Lett.*, vol. 116, no. 6, Feb. 2020, Art. no. 060501.

[32] Q. W. Lin and X. Y. Zhang, "Differential rectifier using resistance compression network for improving efficiency over extended input power range," *IEEE Trans. Microw. Theory Techn.*, vol. 64, no. 9, pp. 2943–2954, Sep. 2016.

[33] T. Ngo, A.-D. Huang, and Y.-X. Guo, "Analysis and design of a reconfigurable rectifier circuit for wireless power transfer," *IEEE Trans. Ind. Electron.*, vol. 66, no. 9, pp. 7089–7098, Sep. 2019.

[34] F. Mirzavand, V. Nayyeri, M. Soleimani, and R. Mirzavand, "Efficiency improvement of WPT system using inexpensive auto-adaptive impedance matching," *Electron. Lett.*, vol. 52, no. 25, pp. 2055–2057, Dec. 2016.

[35] A. M. Hawkes, A. R. Katko, and S. A. Cummer, "A microwave metamaterial with integrated power harvesting functionality," *Appl. Phys. Lett.*, vol. 103, no. 16, Sep. 2013, Art. no. 163901.

[36] P. Xu, S.-Y. Wang, and W. Geyi, "Design of an effective energy receiving adapter for microwave wireless power transmission application," *AIP Adv.*, vol. 6, no. 10, Oct. 2016, Art. no. 105010.

[37] D. F. Sievenpiper, J. H. Schaffner, H. J. Song, R. Y. Loo, and G. Tangonan, "Two-dimensional beam steering using an electrically tunable impedance surface," *IEEE Trans. Antennas Propag.*, vol. 51, no. 10, pp. 2713–2722, Oct. 2003.

[38] J. Guo, H. Zhang, and X. Zhu, "Theoretical analysis of RF-DC conversion efficiency for class-F rectifiers," *IEEE Trans. Microw. Theory Techn.*, vol. 62, no. 4, pp. 977–985, Apr. 2014.

Long Li (Senior Member, IEEE) received the B.E. and Ph.D. degrees in electromagnetic fields and microwave technology from Xidian University, Xi'an, China, in 1998 and 2005, respectively.

He was a Senior Research Associate with the Wireless Communications Research Center, City University of Hong Kong, Hong Kong, in 2006. He visited Tohoku University, Sendai, Japan, as a JSPS Fellow, from 2006 to 2008. He was a Senior Visiting Scholar with The Pennsylvania State University, State College, PA, USA, in 2014. He is currently a Professor with the School of Electronic Engineering, Xidian University. He is also the Director of the Key Laboratory of High-Speed Circuit Design and Electromagnetic Compatibility (EMC), Ministry of Education, and the Dean of Hai-Tang No.9 Academy of Xidian University. He has authored or coauthored over 100 articles in journals. He holds more than 20 patents. His research interests include metamaterials/metasurfaces, antennas and microwave devices, field-circuit collaborative design and EMC, wireless power transfer and harvesting technology, and orbital angular moment (OAM) vortex waves.

Prof. Li is also a Senior Member of Chinese Institute of Electronics (CIE). He received the Nomination Award of National Excellent Doctoral Dissertation of China in 2007. He won the Best Paper Award at the International Symposium on Antennas and Propagation in 2008. He received the Program for New Century Excellent Talents in University of the Ministry of Education of China in 2010. He won the First Prize of Awards for Scientific Research Results offered by Shaanxi Provincial Department of Education, China, in 2013. He received the IEEE APS Raj Mittra Travel Grant Senior Researcher Award in 2015. He received the Shaanxi Youth Science and Technology Award in 2016 and the Outstanding Young Foundation of Shaanxi Province of China. He also received the Japan Society for Promotion of Science (JSPS) Postdoctoral Fellowship. He is also the TPC Co-Chair of Asia-Pacific Conference on Antennas and Propagation (APCAP) 2017 and the General Co-Chair of Asian Wireless Power Transfer Workshop (AWPT) 2019. He is also the Vice-President of the MTT-Chapter of the IEEE Xi'an Section. He also serves as an Associate Editor for the *ACES Journal* and a Guest Editor for the IEEE J-ERM Special Issue.

Xuanming Zhang received the B.E. and Ph.D. degrees in electromagnetic fields and microwave technology from Xidian University, Xi'an, China, in 2014 and 2020, respectively.

He visited the High Frequency Engineering Group, University of Liverpool, Liverpool, U.K., as a Visiting Student, in 2019. His research interests include metasurfaces design, wireless power transfer, and wireless energy harvesting.

Dr. Zhang received the National Scholarship for doctoral students in 2017, the First Prize of the Key Laboratory of High Speed Circuit Design and Electromagnetic Compatibility (EMC) of Ministry of Education Academic Annual Conference in Xidian University in 2017, and the Honorable Mention in Mathematical Contest in Modeling (MCM) in 2013. He also received funding supported by the China Association for Science and Technology (CAST) Fellowship Scheme.

Chaoyun Song (Member, IEEE) received the B.Eng., M.Sc., and Ph.D. degrees in electrical engineering and electronics from the University of Liverpool (UoL), Liverpool, U.K., in 2012, 2013, and 2017, respectively.

He was a Post-Doctoral Research Associate with UoL from 2017 to 2020. He is currently an Assistant Professor with the School of Engineering and Physical Sciences (EPS), Heriot-Watt University, Edinburgh, U.K. He has published more than 70 articles (including 30 IEEE TRANSACTIONS) in peer-reviewed journals and conference proceedings. He holds two U.S. patents and two U.K. patents. His current research interests include wireless energy harvesting and wireless power transfer technologies, antennas and microwave circuits using novel materials, dielectric material and ionic liquids in RF applications, metamaterials and metasurfaces in RF, energy harvesting, and sensing technologies.

Dr. Song was a recipient of many international awards, such as the BAE Systems Chairman's Award in 2017 for the innovation of next-generation global navigation satellite system antennas. In 2018, he received the highly commended award from the prestigious Institution of Engineering and Technology (IET) Innovation Awards over three categories: "Energy and Power," "Emerging Technologies," and "Young Innovators." He has been a regular Reviewer of more than 25 international journals, including *Nature Communications*, *Applied Physics Letters*, *Nano Energy*, and seven IEEE TRANSACTIONS and a Guest Editor of *Wireless Communications and Mobile Computing*.

Wenzhang Zhang received the M.Sc. degree in electrical engineering and electronics from the University of Liverpool (UoL), Liverpool, U.K., in 2016, where she is currently pursuing the Ph.D. degree in wireless communications and RF engineering.

Her research interests include a metasurface-based antenna and characteristic mode analysis.

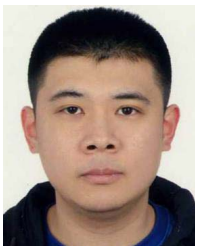

Tianyuan Jia received the B.Eng. degree in telecommunications engineering from Xi'an Jiaotong-Liverpool University (XJTLU), Suzhou, China, in 2012, and the M.Sc. degree in communications and signal processing from Imperial College London, London, U.K., in 2013. He is currently pursuing the Ph.D. degree in electrical engineering and electronics with the University of Liverpool, Liverpool, U.K.

His current research interests include reverberation chamber measurement techniques, 5G over-the-air testing, propagation channel modeling and emulation, electromagnetic compatibility (EMC) testing, statistical electromagnetics, and localization techniques.

Yi Huang (Senior Member, IEEE) received the B.Sc. degree in physics fom Wuhan University, Wuhan, China, in 1984, the M.Sc. (Eng.) degree in microwave engineering from the Nanjing Research Institute of Electronics Technology (NRIET), Nanjing, China, in 1987, and the D.Phil. degree in communications from the University of Oxford, Oxford, U.K., in 1994.

He has been conducting research in the areas of wireless communications, applied electromagnetics, radar, and antennas since 1987. His experience includes three years spent with NRIET as a Radar Engineer and various periods with the University of Birmingham, Birmingham, U.K., the University of Oxford, and the University of Essex, Colchester, U.K., as a member of Research Staff. He was a Research Fellow with British Telecom Labs, London, U.K., in 1994. He joined the Department of Electrical Engineering and Electronics, University of Liverpool, Liverpool, U.K. as a Faculty Member, in 1995, where he is currently a Full Professor of wireless engineering, the Head of the High Frequency Engineering Group, and the Deputy Head of the Department of Electrical Engineering and Electronics. He has published over 350 refereed articles in leading international journals and conference proceedings and authored *Antennas: From Theory to Practice* (John Wiley, 2008) and *Reverberation Chambers: Theory and Applications to Electromagnetic Compatibility (EMC) and Antenna Measurements* (John Wiley, 2016).

Dr. Huang is also a Fellow of Institution of Engineering and Technology (IET) and a Senior Fellow of Higher Education Academy (HEA). He received many research grants from research councils, government agencies, charity, EU, and industry, acted as a consultant to various companies, and served on a number of national and international technical committees. He has been an editor, an associate editor, or a guest editor of five international journals. He has been a Keynote/Invited Speaker and an Organizer of many conferences and workshops (e.g., International Conference on Wireless Communications (WiCom) 2006 and 2010, the IEEE International Workshop on Antenna Technology (iWAT) 2010, Loughborough Antennas & Propagation Conference (LAPC) 2012, and European Conference on Antennas and Propagation (EuCAP) 2018). He is also the Editor-in-Chief of *Wireless Engineering and Technology*, an Associate Editor of the IEEE ANTENNAS AND WIRELESS PROPAGATION LETTERS, U.K., and the Ireland Rep to the European Association of Antenna and Propagation (EurAAP).